Journal Pre-proof

A cell-centered implicit finite difference scheme to study wave propagation in acoustic media: A numerical modelling

Sunita Kumawat, Ajay Malkoti, Sumit Kumar Vishwakarma

PII: S0022-460X(24)00364-X
DOI: https://doi.org/10.1016/j.jsv.2024.118601
Reference: YJSVI 118601

To appear in: *Journal of Sound and Vibration*

Received date : 27 February 2024
Revised date : 8 June 2024
Accepted date : 24 June 2024

Please cite this article as: S. Kumawat, A. Malkoti and S.K. Vishwakarma, A cell-centered implicit finite difference scheme to study wave propagation in acoustic media: A numerical modelling, *Journal of Sound and Vibration* (2024), doi: https://doi.org/10.1016/j.jsv.2024.118601.

A Cell-Centered Implicit Finite Difference Scheme to Study Wave Propagation in Acoustic Media: A Numerical Modelling

Sunita Kumawat[1], Ajay Malkoti[2], Sumit Kumar Vishwakarma[3,*],
[1]Department of Mathematics, BITS-Pilani, Hyderabad Campus, Hyderabad-500078, India,
sunita14kumawat@gmail.com
[2] CSIR-National Geophysical Research Institute, Hyderabad-500007, ajmalkoti@gmail.com
[3]Department of Mathematics, BITS-Pilani, Hyderabad Campus, Hyderabad-500078, India,
sumitkumar@hyderabadbits-pilani.ac.in
*Corresponding author

Abstract

In the present paper, we present a Cell-Centered Implicit Finite Difference (CCIFD) operator-based numerical scheme for the propagation of acoustic waves that is very effective, accurate, and small in size. This scheme requires fewer estimation points than the traditional central difference derivative operator. Any numerical simulation is significantly impacted by the precision of a numerical derivative. Long stencils can deliver excellent accuracy while also minimising numerical anisotropy error. However, a long stencil requires a lot of computational resources, and as these derivatives get bigger, they could start to look physically unrealistic due to contributions from nodes located extremely far, wherein the derivative is local in nature. Furthermore, using such lengthy stencils at boundary nodes may result in errors. The present article investigates a cell-centered fourth order finite difference scheme to model acoustic wave propagation which utilises a lesser number of nodes in comparison to the traditional Central Difference (CD) operator. However, in general the implicit derivative operator has high computational cost and therefore despite its significant advantages it is generally avoided to be implemented in applications. This serves as a motivation for the present paper to explore a technique called CCIFD that significantly decreases the computational expense by nearly fifty percent. Additionally, spectral characterization of the CCIFD derivative operator has been analysed and discussed. Finally, the wave propagation has been numerically simulated in 2-dimensional homogeneous and Marmousi model using CCIFD scheme to validate the applicability and stability of the scheme.

Keywords: Finite-difference, Cell-Centered, Anisotropic, Acoustic waves, Spectral Analysis, Derivative operator.

1. Introduction

An important method for examining the features of seismic waves in complicated media [1–4] is wave equation simulation. In reverse time migration [5] and full waveform inversion [6], wave equation modelling is a crucial building block. Finding practical solutions to the governing equations of acoustic waves is one of the most challenging problems in engineering [7]. These equations, in most cases, form a set of coupled non-linear partial differential equations which may be solved numerically using popular discretization methodologies such as Finite Difference (FD) [8], Finite Volume (FV)[9] and Finite element methods (FEM) [10–13]. However, the field of elastodynamics was dominated by the FD method in its early years [14–17]. The underlying mathematics that forms the foundation of the FD method is relatively simple. This allowed researchers to carry out thorough analyses, such as stability and convergence studies of the algorithms they were developing. Worth to mention that researchers in solid mechanics had been using the finite difference method over the finite element method for many years, although they have generated fairly sophisticated mesh generation techniques [18]. This is due to the fact that standard finite difference methods offer a simpler formulation and implementation than finite element methods as finite difference approach rests on the stencil description. The stencils developed by the forward and the backward finite difference schemes are widely used in one- dimensional problems as compared to the cell centered

schemes while cross stencil, rhombus stencil [19], and radiation stencil are commonly used in higher dimensional problems.

One of the most widely used numerical techniques for simulating wave propagation in intricate velocity models is the finite-difference method. The finite-difference (FD) technique has the advantage of great computing efficiency, small memory footprint, and ease of implementation when compared to the finite-element method, and pseudo-spectral method [20, 21]. As a result, the FD approach has emerged as the most popular numerical technique for simulating wave propagation. Gosselin and Giroux [22] have analysed the frequency-domain finite-difference viscoelastic wave modeling and Flores et al. [23] have used the FD scheme in modelling the seismic wave problem extensively. However, the intrinsic numerical dispersion in FD approaches has an undesirable effect on Full waveform inversion and Reverse time migration results and greatly hinders the simulation accuracy. Hence, a primary obstacle for the FD technique involves controlling numerical dispersion to enhance simulation precision, given the direct correlation between the accuracy of the numerical scheme and the accuracy of the numerical derivative operator. Various numerical derivative operators have been employed in wave propagation, as evidenced in the literature. One such example is the classical central derivative operator, derived from Taylor's series expansion, which is employed in simulating seismic wave fields on a collocated grid [24].

The central difference operator over the staggered grid provides decoupling of even odd modes as well as higher accuracy than conventional operators. It was Dablain [25] who revealed that incorporating high-order approximations for these derivatives is capable of reducing the numerical dispersion. As a result the time marching with higher order approximation enhances the computation amount substantially whereas decreases the stability unfortunately. Thus, in order to control the stability, conventional central difference approximation was adopted for the time spacing and the $2M^{th}$ order finite difference scheme for spatial domain by [26, 27] for discretizing the wave equation. A different category of operator, referred to as an implicit operator, is grounded in the Padé scheme [28]. This operator incorporates both the function's value and the derivative's value, which are available at a given point along with some neighboring points, to estimate the derivative of a function at a specific node. A compact FD scheme of second derivative as discussed in Lele [28] have been introduced in the paper which has the flexibility to be applied on an unstructured mesh. The governing equation is differenced over all the cell centres, including the grid points, as would typically be done in a conventional FD approach, hence the name Cell-Centered Implicit Finite Difference (CCIFD). Several simple test cases have been investigated in this paper to illustrate the development and application of this CCIFD scheme. The numerical results are compared with the analytical solution and the traditional CD schemes. It has been observed that the structured grid with uniform spacing as shown in Fig. 1, the CCIFD is more efficient than traditional FD schemes. It is more stable and needs less resources. However, for curvilinear coordinates or unequally spaced grid lines, the physical domain may need to be transformed to a computational domain where the PDEs are solved after also being transformed.

A better version of finite difference operators is the compact finite difference formulation, or Hermitian formulation [29–31]. It is a numerical method used for estimating the finite difference approximations. These approximations have better dispersive error and dissipative error properties than explicit schemes due to compact stencil size for hyperbolic problems and are preferable in terms of accuracy. The downside of compact schemes is that they are implicit and demand the solution of a diagonal matrix system for analyzing function value or derivatives at all grid-point locations [32, 33]. Due to the optimal stability condition, compact schemes are more suited as numerical solvers for various well-known equations. This paper deals with a compact schemes that necessitate the value of the function and its derivative at a nodal point and its neighbouring point in order to approximate the derivative of the function at the node i (in particular, we have considered the nodes with fractional step size) and resulting in solving a pentadiagonal matrix to get the derivative of a function at i^{th} node. The accuracy of the numerical derivative approximated by the cell-centered scheme is analysed by the Fourier transformation. Furthermore, a comparsion in numerical and exact derivative is done by the means of a suitable 2D and 3D plot showing the anisotropy in the numerical scheme.

In the formulation presented in the subsequent section the nodes on which the derivatives are evaluated are staggered by a half-cell ($h/2$) from the nodes on which the function values are prescribed. Such grid configuration arises naturally from a finite-volume discretization of conservation equations. As shown below, the cell-centered schemes have better resolution

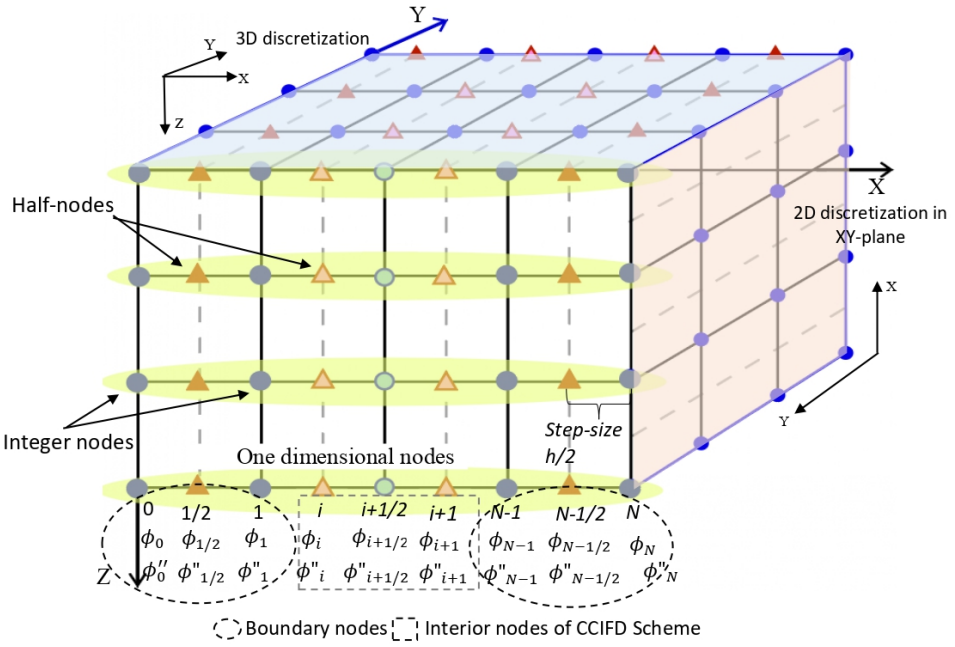

Figure 1: 3D Grid used for evaluating the derivative operator for the cell-centered implicit scheme used for the numerical simulation.

characteristics for wavenumbers (k) near π than the traditional FD scheme [28, 34]. It is important to highlight that the employment of cell-centered schemes for differentiation necessitates the use of accurate interpolation methods. In our analysis and simulation tasks in 2-dimensional domains, we opted for a fourth-order accurate pentadiagonal cell-centered implicit spatial derivative operator. To enhance its computational efficiency, we have introduced a method based on LDM^T decomposition [35] followed by a pre-decomposition technique. This approach significantly reduces the computational cost. Additionally, we conducted a comparative analysis with various other schemes, examining accuracy, numerical anisotropic error, and associated computational costs. Finally, we implemented the CCIFD scheme to simulate wave propagation in both homogeneous and Marmousi models.

2. Formulation: Theory and the Cell-Centered Implicit Finite Difference (CCIFD) Scheme

2.1. *The wave equation and discretization*

Let us suppose that the acoustic medium be evenly discretized along x, y, and z directions with a total number of nodes being N, L, M respectively, as shown in Figure 1. The governing equation of motion for the propagation of wave field $\Phi(\mathbf{x}, t)$ at a given time instance t and location, $\mathbf{x} = (x, y, z)$ in the given medium is given by

$$\partial_t^2 \Phi(\mathbf{x}, t) = c^2(\mathbf{x}) \nabla^2 \Phi(\mathbf{x}, t) \tag{1}$$

where $\nabla^2 = \partial_x^2 + \partial_y^2 + \partial_z^2$ is the Laplacian operator; $c(\mathbf{x})$ is the velocity of the medium. The medium is uniformly and equally discretized along x, y, and z directions, and the nodes have been indicated by the subscript indices i, j, and k, respectively.

The 2-dimensional and 3-dimensional discretized form of equation 1 have been presented as:

$$\Phi_{i,k}^{n+1} = 2\Phi_{i,k}^{n} - \Phi_{i,k}^{n-1} + c^2(i,k)\Delta t^2 (D_x^2 \Phi_{i,k}^{n} + D_z^2 \Phi_{i,k}^{n}) \tag{2}$$

$$\Phi_{i,j,k}^{n+1} = 2\Phi_{i,j,k}^{n} - \Phi_{i,j,k}^{n-1} + c^2(i,j,k)\Delta t^2 (D_x^2 \Phi_{i,j,k}^{n} + D_y^2 \Phi_{i,j,k}^{n} + D_z^2 \Phi_{i,j,k}^{n}) \tag{3}$$

where the subscript indices i, j, and k denotes the i^{th}, j^{th}, and k^{th} nodes in the direction of $x-$, $y-$, and $z-$ directions respectively. The superscript $(n+1)$, n, and $(n-1)$ denotes the future-step, present-step and past-step in the time domain. Also, $D_x^2 = \partial_x^2$,$D_y^2 = \partial_y^2$, and $D_z^2 = \partial_z^2$. It is to be noted that the second order derivative with respect to time has been replaced with a central difference scheme of order 2.

2.2. Numerical Differentiation

The finite difference approximation to the derivative of a function, say $\phi(x)$ at some point x_i in the computational domain i.e. $\phi'(x_i)$ or $\phi''(x_i)$ or higher order derivatives, depends largely on the suitable combination of the sample function values at the neighbouring points. It should be noted that explicit schemes for accessing derivative, such as second-order and fourth-order central difference, employ the set of points locally to approximate the derivative using $\{\phi_{i-1}, \phi_i, \phi_{i+1}\}$ and $\{\phi_{i-2}, \phi_{i-1}, \phi_i, \phi_{i+1}, \phi_{i+2}\}$ respectively. However, the spectral method utilizes all the nodal points in the domain to approximate the derivative and creates the global dependencies of the nodal points for determining the derivatives.

In the present article, an implicit scheme has been presented for derivatives at mid-cell locations, for accurate interpolation, and for spectral-like filtering. Further, this compact finite difference scheme for the second derivatives on a cell-centered mess has been used to solve the wave equation. In the formulation presented below, the nodes on which the derivatives are evaluated are staggered by a half-cell from the nodes on which the function values are prescribed. The position of the nodes is given by $x_i = i\Delta x = ih/2$; h being the step size of the integer nodes in the spatial domain, $i = 0, 0.5, 1, \cdots, n$ and the function value at i^{th} node is $\phi_i = \phi(x_i)$. A generalized relation between $\boldsymbol{\phi}$, and $\boldsymbol{\phi''}$ can be established as following:

$$A\boldsymbol{\phi''} = \frac{1}{h^2} B\boldsymbol{\phi} \tag{4}$$

where $\boldsymbol{A}$ and $\boldsymbol{B}$ are matrices. The values of the function at every node in the neighborhood of the point i, including node i, are needed to compute the explicit derivative at the specified node i (say) using central difference scheme. In this case, $\boldsymbol{A}$ is an identity matrix, and $\boldsymbol{B}$ is a diagonally banded matrix. This is not difficult to derive using Taylor's series expansion in the second-order derivative operator as defined below.

$$\frac{\partial^2 \phi(x_i)}{\partial^2 x} = \frac{1}{h^2} \Sigma_{l=-L}^{L} c_l \ \phi(x_{i+l}) \tag{5}$$

In view of equation 5, the matrix A and B for the central difference of order 2, 4, 6, and 8 have been provided in Appendix A.

On the other hand, the implicit finite difference operator, in contrast, requires values of the function and its derivative at all of the nodes in the neighbourhood of i^{th} node. It results in an implicit relationship between the derivative's values and the function's values. One such implicit finite difference scheme has been suggested by [28] as given by

$$\phi_i'' + \delta\,(\phi_{i-1}'' + \phi_{i+1}'') + \gamma\,(\phi_{i-2}'' + \phi_{i+2}'') = \frac{4}{h^2}\left(p\ \frac{\phi_{i+1/2} - 2\phi_i + \phi_{i-1/2}}{h^2} + q\ \frac{\phi_{i+3/2} - 2\phi_i + \phi_{i-3/2}}{9h^2} + r\ \frac{\phi_{i+5/2} - 2\phi_i + \phi_{i-5/2}}{25h^2}\right) \tag{6}$$

Equation 6 presents a Cell-Centered Implicit Finite Difference (CCIFD) scheme for the second order derivatives which has been employed to approximate the second derivatives appearing in the wave equation. The scheme outlined in equation 6 calculates the second-order derivative at a particular node i by applying a linear combination of values at both integer and non-integer neighboring nodes, as detailed in Equation B.2.1 [28].

In view of 4 this scheme gives a banded structure to the matrices $\boldsymbol{A}$ and $\boldsymbol{B}$ unlike to central difference numerical derivative. The coefficients (δ, γ) on the left hand side and (p, q, r) on the right hand side of equation 6 needs to be calculated with the necessary precision. However, the accuracy may be enhanced by increasing the number of nodes on either side. We use the Taylor series to extend each side of equation 6 to find the coefficients $\{p, q, r, \delta, \gamma\}$, which are then compared to the coefficients of the corresponding derivative both sides. The comparison leads to the following

relationship between the coefficients for h^j; $j = 0, 2, 4, 6, 8$ to find the unknowns $\{p, q, r, \delta, \gamma\}$

$$p + q + r - 2\delta - 2\gamma - 1 = 0 : (h^0, \phi^2) \tag{7a}$$
$$\frac{8}{4! \times 2^4}(p + 3^2 q + 5^2 r) - \frac{2}{2!}(\delta + 2^2\gamma) = 0 : (h^2, \phi^4) \tag{7b}$$
$$\frac{8}{6! \times 2^6}(p + 3^4 q + 5^4 r) - \frac{2}{4!}(\delta + 2^4\gamma) = 0 : (h^4, \phi^6) \tag{7c}$$
$$\frac{8}{8! \times 2^8}(p + 3^6 q + 5^6 r) - \frac{2}{6!}(\delta + 2^6\gamma) = 0 : (h^6, \phi^8) \tag{7d}$$
$$\frac{8}{10! \times 2^{10}}(p + 3^8 q + 5^8 r) - \frac{2}{8!}(\delta + 2^8\gamma) = 0 : (h^8, \phi^{10}) \tag{7e}$$

The coefficients $\{p, q, r, \delta, \gamma\}$ for numerical derivative operators achieving accuracy of order $O(h^n)$ can be determined by solving the corresponding equations in 7(a) to 7(e). In order to meet the accuracy with the least computation time and minimal truncation error, a fourth-order scheme has been developed using the above set of equations, the coefficients of which are given as

$$\{p, q, r, \delta, \gamma\} = \{\frac{19}{8}, \frac{-49}{24}, 0, \frac{-1}{3}, 0\} \tag{8}$$

Rewriting equations 7a and 7b, we have,

$$p = \frac{1}{8}(9 - 30\delta - 174\gamma + 16r) \tag{9}$$
$$q = \frac{1}{8}(-1 + 46\delta + 190\gamma - 24r) \tag{10}$$

The Truncation error associated with the fourth-order Cell Centered Implicit Finite Difference (CCIFD) scheme may be evaluated by comparing the coefficients of $h^4\phi_i^{(6)}$ on both sides of the equation 6. i.e.,
The truncation error (T.E.) maybe given as

$$\begin{aligned} &= \left(\frac{8}{6! \times 2^6}(p + 3^4 q + 5^4 r) - \frac{2}{4!}(\delta + 2^4\gamma)\right) h^4\phi_i^{(6)} \\ &= \left(\frac{1}{5760}(\frac{1}{8}(9 - 30\delta - 174\gamma + 16r) + 3^4(\frac{1}{8}(-1 + 46\delta + 190\gamma - 24r)) + 5^4 r) - \frac{2}{4!}(\delta + 2^4\gamma)\right) h^4\phi_i^{(6)} \\ &= \frac{1}{1920}(3 + 6\delta + 1962\gamma - 128r) h^4\phi_i^{(6)} \end{aligned}$$

On using, $\delta = -1/3$, $\gamma = 0$, $r = 0$ in the above expression the truncation error reduces to $\frac{1}{1920}\mathbf{h^4}\boldsymbol{\phi}_\mathbf{i}^{(\mathbf{6})}$.

2.3. Numerical derivative at boundary points

The aforementioned formulation is applicable exclusively to interior nodes where the finite difference stencil maintains symmetry. It is important to highlight that on the boundary of the given region, there are nodes only on one side of the stencil, resulting in its asymmetry, as illustrated in Figure 1. The absence of nodes on the other side of the boundary area necessitates a reformulation of the implicit finite difference scheme, as depicted in the Table 1 below.
Let us now consider the implicit scheme for $i = 0.5$ as given in Table 1.

$$\phi''_{0.5} + \delta\phi''_{1.5} = \frac{4}{h^2}(a_1\phi_{0.5} + a_2\phi_1 + a_3\phi_{1.5} + \text{.....} + a_n\phi_{4.5}) \tag{11}$$

Using the Taylor series expansion on the left hand side of above equation gives

$$\begin{aligned} \phi''_{0.5} + \delta\phi''_{1.5} = (\phi''_0 + \frac{(h/2)\phi'''_0}{1!} + \frac{(h/2)^2\phi^{iv}_0}{2!} + \frac{(h/2)^3\phi^{v}_0}{3!} + \frac{(h/2)^4\phi^{vi}_0}{4!} + \cdots) + \\ \delta(\phi''_0 + \frac{(3h/2)\phi'''_0}{1!} + \frac{(3h/2)^2\phi^{iv}_0}{2!} + \frac{(3h/2)^3\phi^{v}_0}{3!} + \frac{(3h/2)^4\phi^{vi}_0}{4!} + \cdots) \end{aligned} \tag{12}$$

and, the right hand side gives

$$\frac{4}{h^2}(a_1\phi_{0.5} + a_2\phi_1 + a_3\phi_{1.5} + \ldots\ldots\ldots + a_9\phi_{4.5}) =$$
$$\frac{4}{h^2}\Big\{a_1(\phi_0 + \frac{(h/2)\phi_0'}{1!} + \frac{(h/2)^2\phi_0''}{2!} + \frac{(h/2)^3\phi_0'''}{3!} + \cdots) + a_2(\phi_0 + \frac{h\phi_0'}{1!} + \frac{h^2\phi_0''}{2!} + \frac{h^3\phi_0'''}{3!} + \cdots) +$$
$$a_3(\phi_0 + \frac{(3h/2)\phi_0'}{1!} + \frac{(3h/2)^2\phi_0''}{2!} + \frac{(3h/2)^3\phi_0'''}{3!} + \cdots) + \cdots + a_9(\phi_0 + \frac{(9h/2)\phi_0'}{1!} + \frac{(9h/2)^2\phi_0''}{2!} + \frac{(9h/2)^3\phi_0'''}{3!} + \cdots)\Big\} \tag{13}$$

In order to find the numerical values of the unknowns $a_1, a_2, \cdots, \delta$ we compare the coefficients of $\phi_0, \phi_0', \phi_0'', \phi_0''', \phi_0^{iv}, \cdots, \phi_0^{ix}$ both sides, we get

$$a_1 + a_2 + a_3 + a_4 + a_5 + a_6 + a_7 + a_8 + a_9 = 0 \tag{14a}$$
$$(1/2)a_1 + a_2 + (3/2)a_3 + 2a_4 + (5/2)a_5 + 3a_6 + (7/2)a_7 + 4a_8 + (9/2)a_9 = 0 \tag{14b}$$
$$(1/2)^2a_1 + a_2 + (3/2)^2a_3 + 2^2a_4 + (5/2)^2a_5 + 3^2a_6 + (7/2)^2a_7 + 4^2a_8 + (9/2)^2a_9 = \frac{(1+\delta)2!}{4} \tag{14c}$$
$$(1/2)^3a_1 + a_2 + (3/2)^3a_3 + 2^3a_4 + (5/2)^3a_5 + 3^3a_6 + (7/2)^3a_7 + 4^3a_8 + (9/2)^3a_9 = \frac{(1+3\delta)3!}{2\cdot 4} \tag{14d}$$
$$(1/2)^4a_1 + a_2 + (3/2)^4a_3 + 2^4a_4 + (5/2)^4a_5 + 3^4a_6 + (7/2)^4a_7 + 4^4a_8 + (9/2)^4a_9 = \frac{(1+3^2\delta)4!}{2^2\cdot 2!\cdot 4} \tag{14e}$$
$$(1/2)^5a_1 + a_2 + (3/2)^5a_3 + 2^5a_4 + (5/2)^5a_5 + 3^5a_6 + (7/2)^5a_7 + 4^5a_8 + (9/2)^5a_9 = \frac{(1+3^3\delta)5!}{2^3\cdot 3!\cdot 4} \tag{14f}$$
$$(1/2)^6a_1 + a_2 + (3/2)^6a_3 + 2^6a_4 + (5/2)^6a_5 + 3^6a_6 + (7/2)^6a_7 + 4^6a_8 + (9/2)^6a_9 = \frac{(1+3^4\delta)6!}{2^4\cdot 4!\cdot 4} \tag{14g}$$
$$(1/2)^7a_1 + a_2 + (3/2)^7a_3 + 2^7a_4 + (5/2)^7a_5 + 3^7a_6 + (7/2)^7a_7 + 4^7a_8 + (9/2)^7a_9 = \frac{(1+3^5\delta)7!}{2^5\cdot 5!\cdot 4} \tag{14h}$$
$$(1/2)^8a_1 + a_2 + (3/2)^8a_3 + 2^8a_4 + (5/2)^8a_5 + 3^8a_6 + (7/2)^8a_7 + 4^8a_8 + (9/2)^8a_9 = \frac{(1+3^6\delta)8!}{2^6\cdot 6!\cdot 4} \tag{14i}$$
$$(1/2)^9a_1 + a_2 + (3/2)^9a_3 + 2^9a_4 + (5/2)^9a_5 + 3^9a_6 + (7/2)^9a_7 + 4^9a_8 + (9/2)^9a_9 = \frac{(1+3^7\delta)9!}{2^7\cdot 7!\cdot 4} \tag{14j}$$

The solution to the above system of simultaneous equations leads to the solution given by

$$(a_1, a_2, a_3, a_4, a_5, a_6, a_7, a_8, a_9, \delta) =$$
$$(10.007, -116.745, 209.404, -105.043, -3.743, 9.464, -4.225, 0.980, -0.098, -80.105)$$

Boundary Node	**Implicit Scheme**
$i = 0.5$	$\phi_{0.5}'' + \delta\phi_{1.5}'' = \frac{4}{h^2}(a_1\phi_{0.5} + a_2\phi_1 + a_3\phi_{1.5} + \ldots\ldots\ldots + a_n\phi_N)$
$i = 1$	$\phi_1'' + \delta\phi_2'' = \frac{4}{h^2}(a_1\phi_{0.5} + a_2\phi_1 + a_3\phi_{1.5} + \ldots\ldots\ldots + a_n\phi_N)$
$i = 1.5$	$\delta\phi_{0.5}'' + \phi_{1.5}'' + \delta\phi_{2.5}'' = \frac{4}{h^2}(a_1\phi_{0.5} + a_2\phi_1 + a_3\phi_{1.5} + \ldots\ldots\ldots + a_n\phi_N)$
$i = N - 1$	$\delta\phi_{N-2}'' + \phi_{N-1}'' + \delta\phi_N'' = \frac{4}{h^2}(a_1\phi_{0.5} + a_2\phi_1 + a_3\phi_{1.5} + \ldots\ldots\ldots + a_n\phi_N)$
$i = N - 1/2$	$\phi_{N-1/2}'' + \delta\phi_{N+1/2}'' = \frac{4}{h^2}(a_1\phi_{0.5} + a_2\phi_1 + a_3\phi_{1.5} + \ldots\ldots\ldots + a_n\phi_N)$
$i = N$	$\phi_N'' + \delta\phi_{N+1}'' = \frac{4}{h^2}(a_1\phi_{0.5} + a_2\phi_1 + a_3\phi_{1.5} + \ldots\ldots\ldots + a_n\phi_N)$

Table 1: Cell-Centered scheme at boundary nodes

Using the same procedure, the unknown coefficient $(a_1, a_2, a_3, a_4, a_5, a_6, a_7, a_8, a_9, \delta)$ can be determined for other bound-

ary nodes as shown in Table 2. It has been observed that the coefficients for the first three boundary nodes and the final three boundary nodes are identical and have the same weight but have different signs, as can be plainly observed. We can also say that the boundary values for the left and right edges, as indicated in Table 3, are inverted in sign and order from one another.

Boundary Node	a_1	a_2	a_3	a_4	a_5	a_6	a_7	a_8	a_9	δ
$i = 1/2$	10.007	−116.745	209.404	−105.043	−3.743	9.464	−4.225	0.980	−0.098	−80.105
$i = 1$	0.417	3.388	−40.077	72.622	−41.416	5.938	−0.986	0.121	−0.007	−24.777
$i = 3/2$	−0.124	1.457	−2.611	1.291	0.082	−0.138	0.055	−0.012	0.001	−0.012
$i = N - 1$	0.001	−0.012	0.055	−0.138	0.082	1.291	−2.611	1.457	−0.124	−0.012
$i = N - 1/2$	−0.007	0.121	−0.986	5.938	−41.416	72.622	−40.077	3.388	0.417	−24.777
$i = N$	−0.098	0.980	−4.225	9.464	−3.743	−105.043	209.404	−116.745	10.007	−80.105

Table 2: The values of the coefficients at the boundary nodes using fourth-order CCIFD scheme

The implicit scheme, as given by equation 6 for the interior points and the boundary scheme, as given by Table 2, forms a complete numerical scheme for one-dimensional wave equation. In view of equation 4, the matrices A and B for one-dimensional wave can be found in Appendix A, where total number of nodes, $n = 9$ (5 non-integer and 4 integers nodes) and $N = 0.5, 1, 1.5, \cdots 4.5$ has been . However, the scheme may be easily extended for the 2D and 3D models by decomposing the 2D and 3D domains into one-dimensional vectors along the directions of the derivatives (say x) so that we may now perform the derivative operator recursively. The other way to find the second derivative for the entire 2D/3D domain can be formulated globally using Kronecker's product $\otimes$ as given by $[I_M \otimes A]\phi'' = [I_M \otimes B]\phi$ and $[I_L \otimes I_M \otimes A]\phi'' = [I_L \otimes I_M \otimes B]\phi$ for 2D and 3D cases respectively, where the matrices A and B are the same as discussed for the one-dimensional case (Appendix B). The matrices I_L and I_M denote identity matrices of order L and M, respectively. It is worth noting that the resulting matrices for 2D and 3D cases would be $N \times M$ and $N \times M \times L$, respectively.

2.4. Fourier analysis of the derivative operator

A frequently used numerical approach to differentiate some sampled function $\phi(x)$ is utilizing Fast Fourier transforms (FFTs). Equivalently, one differentiates an approximate Fourier series refereed as *spectral differentiation methods*. Fourier analysis initially aimed at representing and interpreting periodic phenomena using the Fourier series and then extending those insights to nonperiodic problems using the Fourier transform. The Fourier transformation aids in understanding the accuracy of the derivative in terms of spectrum properties. In the realm of wavenumbers, one can compare the ability of exact and numerically approximated derivatives to handle higher-order wavenumbers. The Fourier transformation and the inverse Fourier transformation of the function $\phi(x)$ and $\phi(\tilde{k})$ are respectively given by

$$\mathcal{F}(\phi(\mathbf{x})) = \int_{-\infty}^{\infty} e^{-i\mathbf{k}.\mathbf{x}} \phi(\mathbf{x}) d\mathbf{x} \tag{15}$$

$$\phi(\mathbf{x}) = \mathcal{F}^{-1}(\tilde{\phi}(\mathbf{k})) = \frac{1}{2\pi} \int_{-\infty}^{\infty} \tilde{\phi}(\mathbf{k}) e^{i\mathbf{k}.\mathbf{x}} d\mathbf{x} \tag{16}$$

The behavior of the derivative obtained from the numerical scheme 5 requires the Discrete Fourier Transformation (DFT). It could be considered as a function that takes a list of P numbers as input and output rather than referring to sampled values of a continuous signal and sampled values of its Fourier transform.
Let us say $\phi = [\phi_0, \phi_1, \phi_2, \phi_3, ..., \phi_N]$ denotes the N input signals over a domain [0, L], then the one-dimensional Discrete Fourier Transform (DFT) of ϕ denoted by $\tilde{\phi}$ is defined as,

$$\tilde{\phi}_j = \mathcal{F}(\phi) \quad = \sum_{p=0}^{N} \phi_p e^{i\frac{-2\pi jp}{N}}; j = 0, 1, 2, ..., N \tag{17}$$

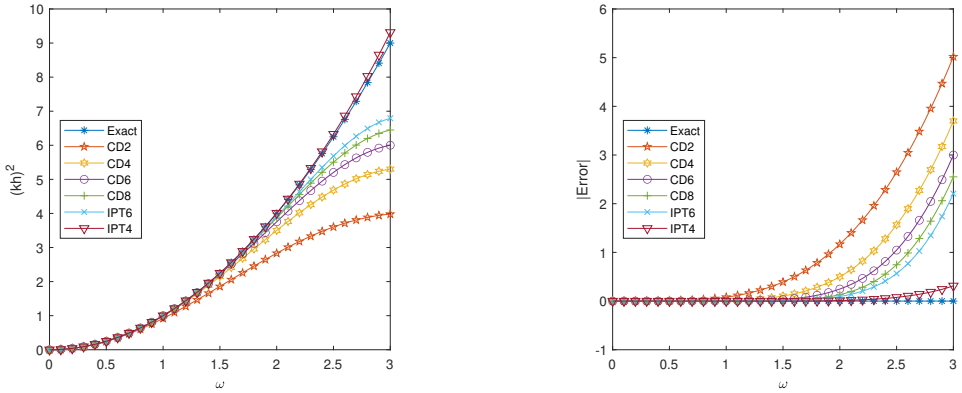

(a) (b)

Figure 2: Comparison of the Implicit derivative operator with various central difference derivative operators (a) angular velocity versus numerical wavenumber. (b) Absolute error between the exact wavenumber and various Central difference wavenumber, implicit derivative wavenumber versus angular velocity.

Similarly, the inverse DFT is defined as,

$$\phi_p = \mathcal{F}^{-1}(\tilde{\phi}) = \frac{1}{N}\sum_{j=0}^{N} \tilde{\phi}_j e^{i\frac{2\pi jp}{N}}; p = 0, 1, 2, ..., N \tag{18}$$

Let k^2_{exact} denotes the exact (analytical) solution of the differential equation (Helmholtz equation). The harmonic form of the solution of equation 1 can be expressed in the form

$$\Phi(\mathbf{x}, t) = \phi(\mathbf{x})e^{i\omega t} \tag{19}$$

Substituting the above expression in equation 1, it reduces to

$$\left(\nabla^2 + \frac{\omega^2}{c^2}\right)\phi = 0$$

which gives,

$$\left(\nabla^2 + k^2_{exact}\right)\phi = 0; k^2_{exact} = \frac{\omega^2}{c^2}$$

which is known as the Helmholtz equation. Applying Fourier transformation to the Helmholtz equation, we get

$$\mathcal{F}\{\nabla^2\phi\} + k^2_{exact}\mathcal{F}\{\phi\} = 0 \tag{20}$$

which implies to

$$((-ik_x)^2 + (-ik_y)^2 + (-ik_z)^2)\tilde{\phi} + k^2_{exact}\tilde{\phi} = 0 \tag{21}$$

i.e.,

$$(-ik)^2\tilde{\phi} + k^2_{exact}\tilde{\phi} = 0; k^2 = k_x^2 + k_y^2 + k_z^2 \tag{22}$$

Finally,

$$k^2_{exact} = k^2; \tag{23}$$

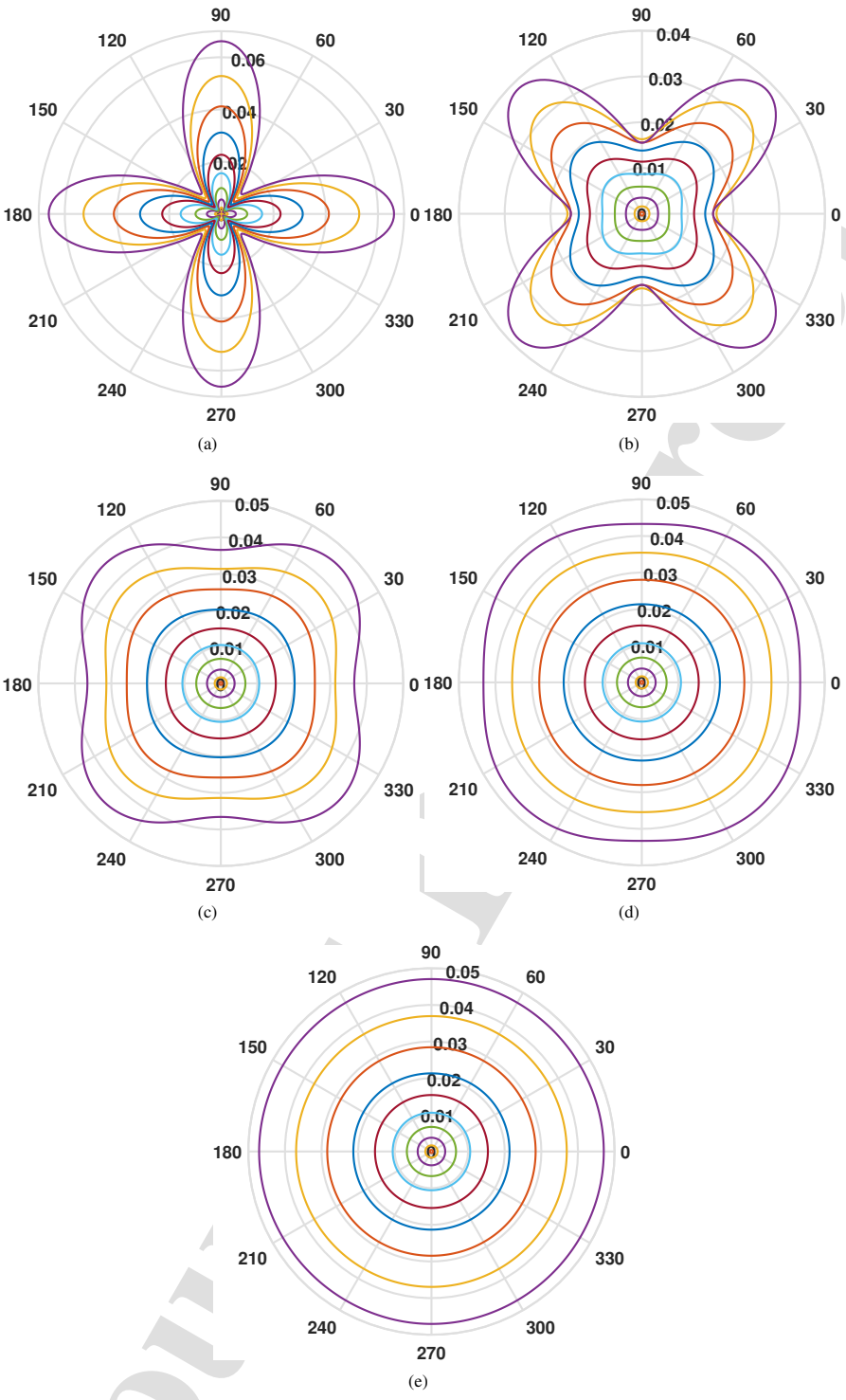

Figure 3: Two-dimensional polar plots reflecting the error in phase velocity (a) Central difference of order 2, (b) Central difference of order 4, (c) Central difference of order 6, (d) Central difference of order 8, (e) CCIFD of order 4.

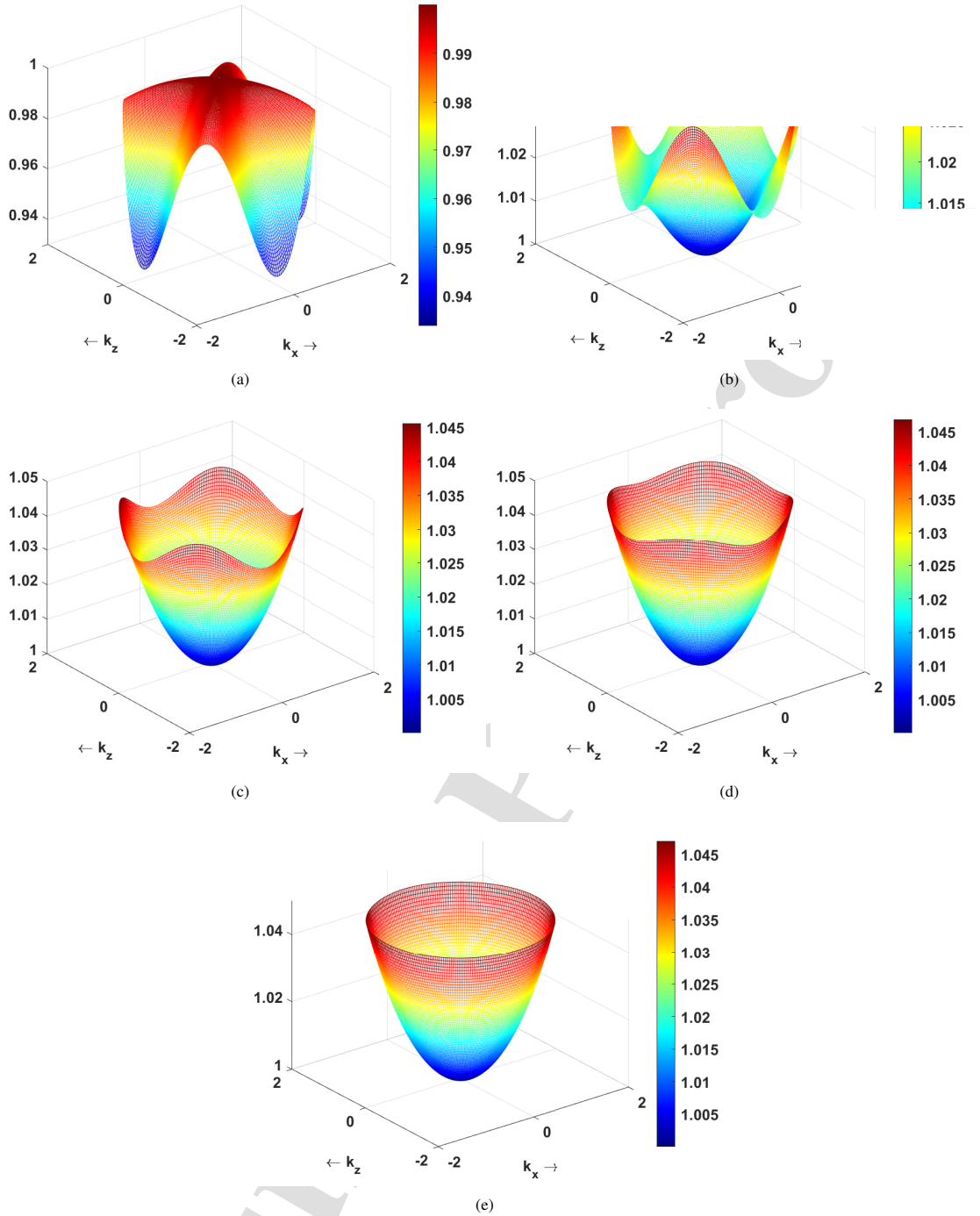

Figure 4: 3D surface plots for the relative phase velocity for various schemes. Subplots (a-d) Central difference of order 2, 4, 6, 8 (e) CCIFD respectively.

2.5. *Approximate wavenumbers for Central difference schemes and CCIFD*

A $2L^{th}$ order central difference formula for approximating second order derivative in 3D Euclidean space is given by

$$\frac{\partial^2\phi}{\partial x^2} = \frac{1}{h^2}\left(d_0\phi_{k,l,m} + \sum_{n=1}^{L} d_n\left(\phi_{k-n,l,m} + \phi_{k+n,l,m}\right)\right), \tag{24}$$

$$\frac{\partial^2\phi}{\partial y^2} = \frac{1}{h^2}\left(d_0\phi_{k,l,m} + \sum_{n=1}^{L} d_n\left(\phi_{k,l-n,m} + \phi_{k,l+n,m}\right)\right), \tag{25}$$

$$\frac{\partial^2\phi}{\partial z^2} = \frac{1}{h^2}\left(d_0\phi_{k,l,m} + \sum_{n=1}^{L} d_n\left(\phi_{k,l,m-n} + \phi_{k,l,m+n}\right)\right). \tag{26}$$

Using equation 17, the Discrete Fourier Transformation (DFT) of the single mode of wave in three Dimensional space ($p = p_1, p_2, p_3$ and $j = k, l, m$ along x, z, y respectively) is given by,

$$\mathcal{F}(\phi_{k,l,m}) = \tilde{\phi}_{p_1,p_2,p_3} e^{\frac{-i2\pi k p_1}{N}} e^{\frac{-i2\pi l p_2}{L}} e^{\frac{-i2\pi m p_3}{M}} \tag{27}$$

Employing equation 27 on $\nabla^2(\phi)$ and using equations 24-26, gives

$$\mathcal{F}(\nabla^2\phi)\Big|_{(k,l,m)} = \frac{3}{h^2} d_0 \tilde{\phi}_{p_1,p_2,p_3} e^{-i2\pi\left(\frac{kp_1}{N}+\frac{lp_2}{L}+\frac{mp_3}{M}\right)}$$
$$+ \frac{1}{h^2}\Bigg(\sum_{n=1}^{L} d_n \tilde{\phi}_{p_1,p_2,p_3} e^{-i2\pi\left(\frac{(k-n)p_1}{N}+\frac{lp_2}{L}+\frac{mp_3}{M}\right)} + \tilde{\phi}_{p_1,p_2,p_3} e^{-i2\pi\left(\frac{(k+n)p_1}{N}+\frac{lp_2}{L}+\frac{mp_3}{M}\right)} + \tilde{\phi}_{p_1,p_2,p_3} e^{-i2\pi\left(\frac{kp_1}{N}+\frac{(l-n)p_2}{L}+\frac{mp_3}{M}\right)} +$$
$$\tilde{\phi}_{p_1,p_2,p_3} e^{-i2\pi\left(\frac{kp_1}{N}+\frac{(l+n)p_2}{L}+\frac{mp_3}{M}\right)} + \tilde{\phi}_{p_1,p_2,p_3} e^{-i2\pi\left(\frac{kp_1}{N}+\frac{lp_2}{L}+\frac{(m-n)p_3}{M}\right)} + \tilde{\phi}_{p_1,p_2,p_3} e^{-i2\pi\left(\frac{kp_1}{N}+\frac{lp_2}{L}+\frac{(m+n)p_3}{M}\right)}\Bigg)$$

which further gives,

$$\mathcal{F}(\nabla^2\phi)\Big|_{(k,l,m)} = \frac{3}{h^2}\tilde{\phi}_{p_1,p_2,p_3} e^{-i2\pi\left(\frac{kp_1}{N}+\frac{lp_2}{L}+\frac{mp_3}{M}\right)}\left(d_0 + \frac{2}{h^2}\sum_{n=1}^{L} d_n\left(\cos\left(\frac{2\pi n p_1}{N}\right) + \cos\left(\frac{2\pi n p_2}{N}\right) + \cos\left(\frac{2\pi n p_3}{N}\right)\right)\right) \tag{28}$$

We know from Helmholtz equation,

$$\left(\nabla^2 + k^2_{approx}\right)\phi = 0; k^2_{approx} = \tilde{k}_x^2 + \tilde{k}_y^2 + \tilde{k}_z^2$$

On applying Discrete Fourier Transformation (DFT) to the above equation,

$$\mathcal{F}\left(\nabla^2\phi) + k^2_{approx}\mathcal{F}(\phi\right) = 0 \tag{29}$$

Using equation 28, in equation 29 we have,

$$\frac{3}{h^2} e^{-i2\pi\left(\frac{kp_1}{N}+\frac{lp_2}{L}+\frac{mp_3}{M}\right)}\left(d_0 + \frac{2}{h^2}\sum_{n=1}^{L} d_n\left(\cos\left(\frac{2\pi n p_1}{N}\right) + \cos\left(\frac{2\pi n p_2}{N}\right) + \cos\left(\frac{2\pi n p_3}{N}\right)\right)\right)\tilde{\phi}_{p_1,p_2,p_3} + k^2_{approx}\tilde{\phi}_{p_1,p_2,p_3} = 0 \tag{30}$$

Now using spherical coordinate system, $p_1 = p\cos\theta\sin\phi$, $p_2 = p\sin\theta\sin\phi$, $p_3 = p\cos\phi$ equation 30 becomes,

$$k^2_{approx} = \frac{1}{h^2}\left(d_0 + 2\sum_{n=1}^{L} d_n\left(\cos\left(\frac{2\pi n p\cos\theta\sin\phi}{N}\right)\right)\right) + \frac{1}{h^2}\left(d_0 + 2\sum_{n=1}^{L} d_n\left(\cos\left(\frac{2\pi n p\sin\theta\sin\phi}{L}\right)\right)\right) +$$
$$\frac{1}{h^2}\left(d_0 + 2\sum_{n=1}^{L} d_n\left(\sin\left(\frac{2\pi n p\cos\phi}{M}\right)\right)\right)$$

Hence,

$$\tilde{k_x}^2 = \frac{1}{h^2}\left[d_0 + 2\sum_{n=1}^{L} d_n\left\{\cos\left(\frac{2\pi n p\cos\theta\sin\phi}{N}\right)\right\}\right] \tag{31a}$$

$$\tilde{k_y}^2 = \frac{1}{h^2}\left[d_0 + 2\sum_{n=1}^{L} d_n\left\{\cos\left(\frac{2\pi n p\sin\theta\sin\phi}{L}\right)\right\}\right] \tag{31b}$$

$$\tilde{k_z}^2 = \frac{1}{h^2}\left[d_0 + 2\sum_{n=1}^{L} d_n\left\{\sin\left(\frac{2\pi n p\cos\phi}{M}\right)\right\}\right] \tag{31c}$$

On substituting $\phi = \pi/2$ (the spherical coordinate system reduces to polar coordinate system corresponding to 2D) in

equation 31, the components of the approximated wavenumber with constant $z-$ component are,

$$\tilde{k_x}^2 = \frac{1}{h^2}\left(d_0 + 2\sum_{n=1}^{L} d_n \cos\left(\frac{2\pi n p \cos\theta}{N}\right)\right), \tag{32a}$$

$$\tilde{k_y}^2 = \frac{1}{h^2}\left(d_0 + 2\sum_{n=1}^{L} d_n \cos\left(\frac{2\pi n p \sin\theta}{L}\right)\right) \tag{32b}$$

Similarly, for $\theta = 0$ in equation 32 gives the approximated wavenumber for 1D case with constant y and z components as shown below,

$$\tilde{k}^2 = \frac{1}{h^2}\left(d_0 + 2\sum_{n=1}^{L} d_n \cos\left(\frac{2\pi n p}{N}\right)\right) \tag{33}$$

Equations 31-33 gives the derivation of Table 3. Whereas Fourier transformation of equation 6 gives the approximated wavenumber for CCIFD given in Table 4.

Dimension	Modified wavenumber	
3	$\tilde{k_x}^2 = \frac{1}{h^2}\left(d_0 + 2\sum_{n=1}^{L} d_l \cos(n\alpha\cos\theta\sin\phi)\right)$, $\tilde{k_y}^2 = \frac{1}{h^2}\left(d_0 + 2\sum_{n=1}^{L} d_l \cos(n\alpha\sin\theta\sin\phi)\right)$, $\tilde{k_z}^2 = \frac{1}{h^2}\left(d_0 + 2\sum_{n=1}^{L} d_l \cos(n\alpha\cos\phi)\right); \alpha = kh$	$; 0 \le \phi \le \pi, 0 \le \theta \le 2\pi$
2	$\tilde{k_x}^2 = \frac{1}{h^2}\left(d_0 + 2\sum_{n=1}^{L} d_l \cos(n\alpha\cos\theta)\right)$, $\tilde{k_y}^2 = \frac{1}{h^2}\left(d_0 + 2\sum_{n=1}^{L} d_l \cos(n\alpha\sin\theta)\right); \alpha = kh$	$; 0 \le \theta \le 2\pi$
1	$\tilde{k}^2 = \frac{1}{h^2}\left(d_0 + 2\sum_{n=1}^{L} d_l \cos(n\omega)\right); \omega = 2\pi p/N$	

Table 3: Approximate wavenumber for central difference derivatives

Dimension	Modified wavenumber
$j = 1$	$\tilde{k}^2 = \frac{-4}{h^2}\left(\frac{2p(1-\cos\omega/2)+\frac{2q}{9}(1-\cos(3\omega/2)+\frac{2r}{25}(1-\cos(5\omega/2))}{2\delta\cos\omega+2\gamma\cos 2\omega+1}\right)$
$j = 2$	$\tilde{k_x}^2 = \frac{-4}{h^2}\left(\frac{2p\left(1-\cos(\frac{1}{2}n\alpha\cos\theta)\right)+\frac{2q}{9}\left(1-\cos(\frac{3}{2}n\alpha\cos\theta)\right)+\frac{2r}{25}\left(1-\cos(\frac{5}{2}n\alpha\cos\theta)\right)}{2\delta\cos(n\alpha\cos\theta)+2\gamma\cos(2n\alpha\cos\theta)+1}\right)$, $\tilde{k_y}^2 = \frac{-4}{h^2}\left(\frac{2p\left(1-\cos(\frac{1}{2}n\alpha\sin\theta)\right)+\frac{2q}{9}\left(1-\cos(\frac{3}{2}n\alpha\sin\theta)\right)+\frac{2r}{25}\left(1-\cos(\frac{5}{2}n\alpha\sin\theta)\right)}{2\delta\cos(n\alpha\sin\theta)+2\gamma\cos(2n\alpha\sin\theta)+1}\right)$
$j = 3$	$\tilde{k_x}^2 = \frac{-4}{h^2}\left(\frac{2p\left(1-\cos(\frac{1}{2}n\alpha\cos\theta\sin\phi)\right)+\frac{2q}{9}\left(1-\cos(\frac{3}{2}n\alpha\cos\theta\sin\phi)\right)+\frac{2r}{25}\left(1-\cos(\frac{5}{2}n\alpha\cos\theta\sin\phi)\right)}{2\delta\cos(n\alpha\cos\theta\sin\phi)+2\gamma\cos(2n\alpha\cos\theta\sin\phi)+1}\right)$ $\tilde{k_y}^2 = \frac{-4}{h^2}\left(\frac{2p\left(1-\cos(\frac{1}{2}n\alpha\sin\theta\sin\phi)\right)+\frac{2q}{9}\left(1-\cos(\frac{3}{2}n\alpha\sin\theta\sin\phi)\right)+\frac{2r}{25}\left(1-\cos(\frac{5}{2}n\alpha\sin\theta\sin\phi)\right)}{2\delta\cos(n\alpha\sin\theta\sin\phi)+2\gamma\cos(2n\alpha\sin\theta\sin\phi)+1}\right)$ $\tilde{k_z}^2 = \frac{-4}{h^2}\left(\frac{2p\left(1-\cos(\frac{1}{2}n\alpha\cos\phi)\right)+\frac{2q}{9}\left(1-\cos(\frac{3}{2}n\alpha\cos\phi)\right)+\frac{2r}{25}\left(1-\cos(\frac{5}{2}n\alpha\cos\phi)\right)}{2\delta\cos(n\alpha\cos\phi)+2\gamma\cos(2n\alpha\cos\phi)+1}\right)$

Table 4: Approximate wavenumber for CCIFD

To contrast the modified wavenumbers for a few CD operators and the implicit derivative operator against the exact

derivative operator, Figure 2 (a) is plotted. According to the illustration, the exact derivative operator is parabolic in nature in terms of wavenumber and independent of the angular velocity ω. Whereas a reliance on ω has been discovered for the Central difference and implicit derivative operator, which deviates from the exact wavenumber curves. Furthermore, it can be outlined briefly from the graph that the deviation rate falls off as the order of the CD operators rises. Secondly, it is evident from the figure, the numerical schemes are ill-suited to precisely mimic higher modes since higher values of angular velocity result in a greater variance in the wavenumber for the numerical schemes with the exact wavenumber. This upshot may be attenuated by using a higher-order derivative operator, leading to higher spectral accuracy. The accuracy is also influenced by the type of operator, which could provide the same formal accuracy but better spectral accuracy. For instance, it may happen that the accuracy of the n^{th} order implicit derivative operator is equivalent to that of the m^{th} order CD operator, which can be observed in the paper [26] for $m = 10$ and $n = 6$. .

Figure 2(a) also gives a clear idea that the cell-centered implicit finite difference scheme of order 4 overestimates the exact wavenumber with a marginal difference towards the higher angular velocity wherein IPT6 [26] falls off to match the accuracy. This is to be noted as the derivative in CCIFD are staggered by half cell from the integer nodes on which the function values are prescribed. These grid configuration arise naturally from a finite volume discretization of a conservation equation. That is the reason cell-centered schemes have better resolution characteristics for approximate wavenumbers. It should be further noted that the use of cell-centered schemes for differentiation compels it to use accurate interpolation. Thereby, the resolution characteristic of the interpolation, when combined with that of cell-centered differentiation, determines the optimal resolution characteristic of the overall scheme. The anisotropy of the scheme, and the discussion about the accuracy have been presented in the subsection below. Figure 2b displays the absolute error between the exact and numerically approximated derivative's dispersion curves for each scheme(CDs and implicit scheme).

2.6. Numerical anisotropy

In order to simulate the higher-order multidimensional PDE via numerical schemes, a specific discretization error known as numerical anisotropy is accessible. The spectral analysis can be used for capturing this numerical anisotropy. One may conceptualize this discretization error as fluctuation in the phase velocity ($v_p = \frac{\omega}{k}$) along distinct axes. The phase velocity of the compact numerical scheme can be obtained by discretizing its Fourier transform. The dimensionless phase velocity for 2D and 3D is given by,

$$v' = \frac{v_p}{c} = \frac{2}{C\alpha}\sin^{-1}\left(\frac{h\ C}{2}\sqrt{\tilde{k}_x^2 + \tilde{k}_y^2}\right) \tag{34}$$

$$v' = \frac{v_p}{c} = \frac{2}{C\alpha}\sin^{-1}\left(\frac{h\ C}{2}\sqrt{\tilde{k}_x^2 + \tilde{k}_y^2 + \tilde{k}_z^2}\right) \tag{35}$$

respectively, where $C = \frac{c\Delta t}{\Delta x}$ deontes the CFL number, and k_x, k_y, k_z are given in Table 3 and Table 4; $\alpha = kh$ denotes the number of grids in a wavelength.

Figure 3 demonstrates 2D polar plots depicting the error in the relative phase velocity $1-v'$ at different values of wavenumber for all the numerical schemes. Analogously, to achieve a better understanding of the relative phase velocity and its error, 3D surface plots have been showcased in Figure 4 and Figure 5, respectively.

While handling a numerical simulation, it is pertinent to retrieve that the precision of the relative phase velocity is consequentially effected by the accuracy of the derivative operator. In the case of the continuous domain, relative phase velocity v' is independent of the wave propagation, whereas the dependency of the wave propagation is met while dealing with the numerical simulation. Thus, to check out the precision of accuracy for the numerical schemes, Figure 4 is displayed and observed that the better accuracy for the curves approximates a paraboloid shape. Moreover, a specific impact of the numerical anisotropy is seen on the top of the surface plots showing a non-circular cup of the paraboloid. This can be seen in a better way from Figure 3, exemplifying the numerical anisotropy error. It is clear from Figure 3 that the FD schemes show a distorted nature, whereas an accuracy comparable to the ideal case can be seen for the implicit case showing lesser error.

To study the accuracy level of the relative phase velocity in 3D, Figure 5 is exhibited. As discussed in the 2D case, ideally,

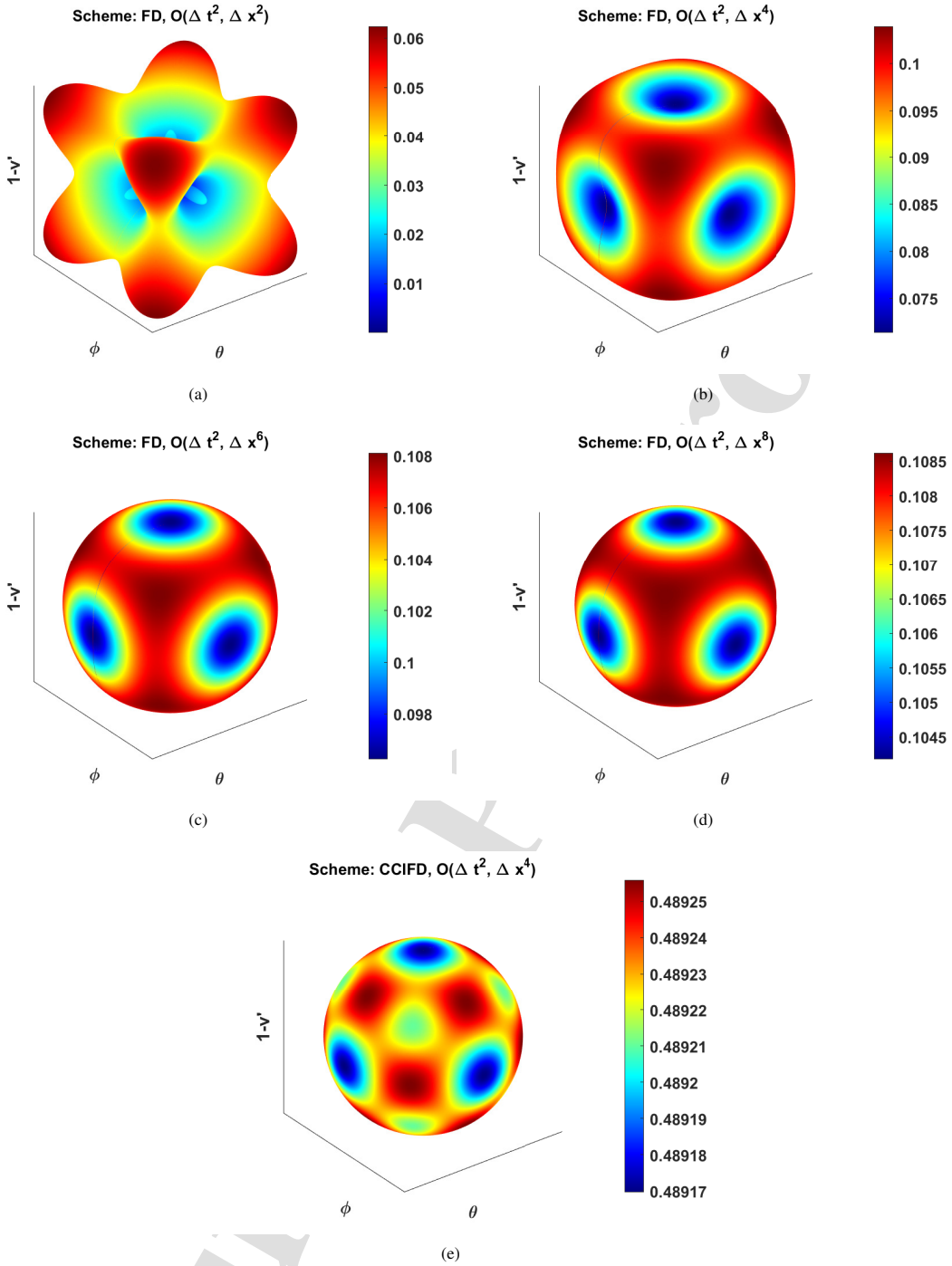

Figure 5: 3D plots representing the error in the phase velocity for central difference of order 2, 4, 6, 8 and CCIFD.

the accuracy level of the scheme is achieved by the spherical nature of the graph. However, due to the existence of the numerical anisotropy, a distorted nature in the spherical shape is seen for all the FD schemes. Analogous to 2D, it has been observed that implicit schemes lead to the least error in the relative phase velocity as the graph is approximately spherical. On observing the 2D and 3D plots, it is self-evident to conclude that, the slightest error is observed along the

coordinate axis i.e. along θ = a $\pi/2$; a = 0, 1, 2,3 and $\phi = 0, \pi$, whereas the maximum error is observed along the diagonal direction for example $\theta = \pi/4$ and $\phi = \pi/4$.

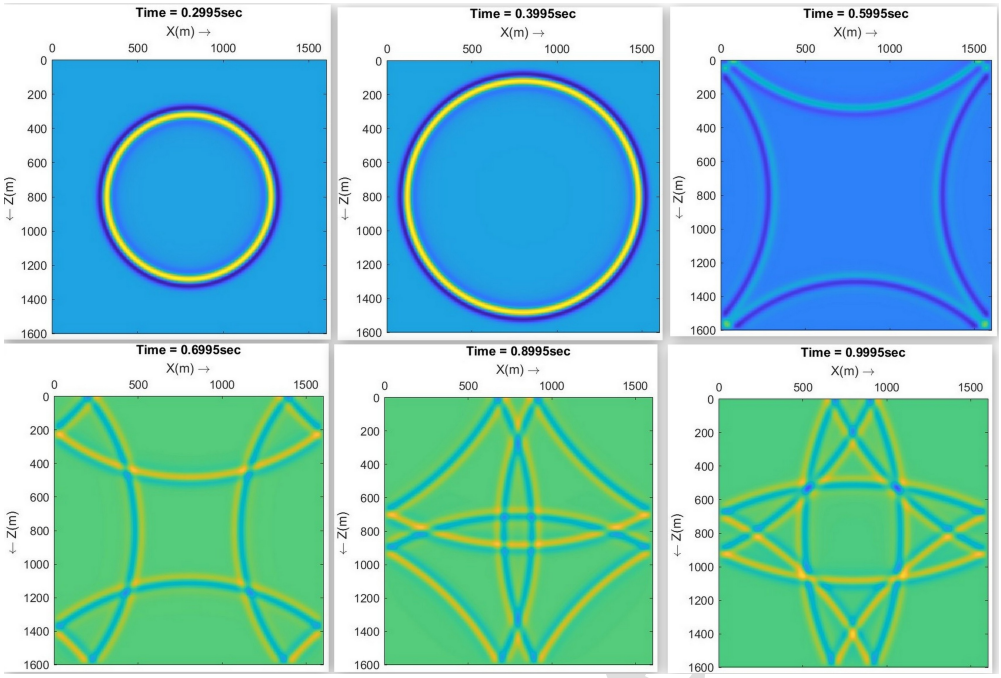

Figure 6: Snapshot of seismic wave propagation in a 2D acoustic media using CCIFD

3. Computational Analysis: FLOPS and LDM^T factorization

The theoretical computational expenses for a numerical operator may be estimated by computing the number of FLOPS used for the fundamental operations (like addition, subtraction, multiplication, and divisions). This subsection will contribute to the evaluation of a number of FLOPS engaged for the various central difference schemes and cell-centered schemes.

Firstly, let us discuss the computational cost for a one-dimensional CD scheme of $2X$ order. In view of equation (5), it is easy to know that, to define a CD scheme of $2X$ order, a stencil with $2X + 1$ nodes is required. In terms of CPU efficiency, a total of $4X + 1$ operations are to be performed at i^{th} node (breaking to $2X$ additions and $2X + 1$ multiplications). Keeping in mind the symmetric nature of the coefficients involved in the second-order differential operator, the number of multiplication may be further reduced to $(3X + 1)N$ operations for N number of nodes. Thus, particularly for a CD scheme of orders 2, 4, 6, and 8 the cost may be enlisted as $4N, 7N, 10N, 13N$.

Let us now discuss the computational cost for the implicit schemes CCIFD. It is worth noting that, as discussed above for CD schemes, we will be evaluating the computing cost for 1D implicit schemes which may be further extended for 2D and 3D schemes. In view of equation 4, the computational cost for the right-hand side operation given by Bf is approximately equal to 7N (breaking up into 4 additions and 3 multiplications). This leads to a system given as $Af'' = g$; g is a column vector. Noting that A is a pentadiagonal system, it can be solved with decomposition methods like LU and LDM^T decomposition. The cost of an arbitrary system $Ax = B$ maybe seen as the sum of cost factorization $10(N - 1)$, forward substitution $4(N - 1)$, and backward substitution $5(N - 1)$. Thus, the total cost for evaluating $A^{-1}Bf$ turns out to be $26(N - 1)$. The 1D cost may be further used to evaluate the cost for 2D and 3D.

Despite the fact that all operations costs are equivalent in theory, while coming to the execution, solely addition and subtraction costs equal one FLOP. Whereas, an individual division operation may cost between two and four FLOPS

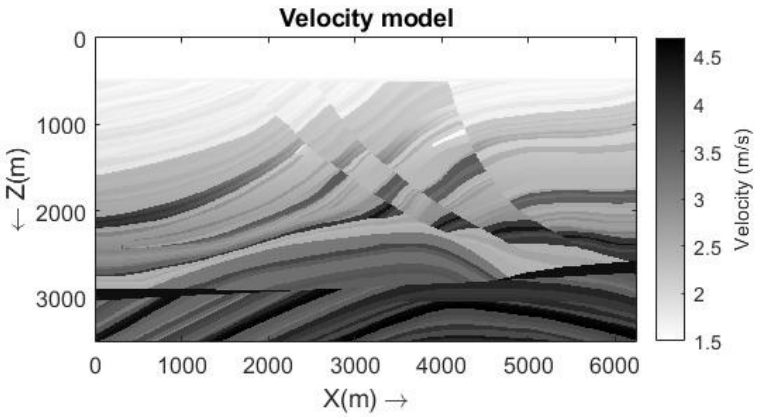

(a)

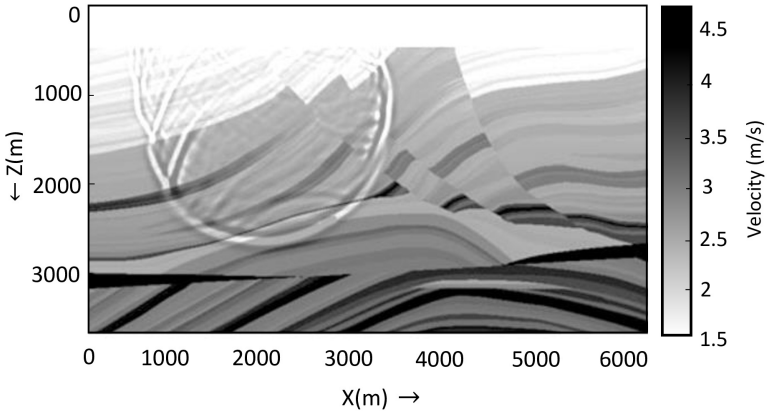

(b)

Figure 7: (a) Velocity model (Marmousi model) used for seismic wave propagation using CCIFD scheme (b) A snapshot of the forward propagating wave

(the industry norm), and a single multiplication typically costs slightly more than one FLOP. It is worth noting that the machine's design, compiler, reliability, etc. are other factors that affect the number of flops. Additionally, timing dependency in repetitions and retrieval of memory patterns are important factors. The computation time for various finite difference schemes has been enlisted in Table 5 and compared with the IPT6 scheme given by [26]. It also includes the computational for the fourth order CCIFD scheme with LU and LDM^T decomposition. It is self-explanatory from Table 5 that the LU decomposition is more expensive compared with the LDM^T decomposition [35](Quarteroni et al., 2010) for both the implicit schemes, and also the CCIFD scheme has comparatively lesser computational time than IPT6 [26]. The existence of the division operation in solving the pentadiagonal matrix and the recurrent computational methods are theoretically responsible for this. Theoretically, this is due to the existence of the division operation in solving the pentadiagonal matrix and the method of recurrent computation for solving the pentadiagonal matrix. It computes two new vectors by breaking down the pentadiagonal matrix into the L and U matrices. This further results in division operations and recursion process, which involves temporal dependency, i.e. i^{th} step dependent on $(i-1)^{th}$. To reduce this time, the

division operations can be minimized using LDM^T factorization given in Appendix B.

Nodes	CD2	CD4	CD6	CD8	IPT 6 (LU)	IPT 6 (LDM^T)	CCIFD(LU)	CCIFD(LDM^T)
Computation time per second								
1000×1000, 2000	8.193	11.405	16.622	20.216	56.486	51.869	55.757	50.981
1000×1000, 4000	16.247	23.337	33.395	40.887	56.761	53.780	56.771	52.230
2000×2000, 2000	40.875	56.798	83.455	101.345	232.901	218.208	230.749	209.066
2000×2000, 4000	82.058	113.590	168.521	201.896	234.353	226.339	233.061	212.219
Normalized computation time per second								
1000×1000, 2000	1.000	1.392	2.028	2.467	6.894	6.330	6.805	6.222
1000×1000, 4000	1.000	1.436	2.055	2.157	3.495	3.311	3.495	3.216
2000×2000, 2000	1.000	1.389	2.041	2.479	5.698	5.340	5.645	5.115
2000×2000, 4000	1.000	1.384	2.053	2.460	2.856	2.758	2.840	2.586

Table 5: Execution time for various number of nodes and time steps

4. Source Point and Numerical Simulation

To demonstrate the application of cell-centered finite difference scheme, we carried out numerical simulations of two types of models, namely the Homogeneous model and the Marmousi model. The specifications of the models are given in Table 6. In order to show how the defined implicit scheme CCIFD may be applied, a computational simulation has been performed for homogeneous and Marmousi model.

	Homogeneous Model	Marmousi Model
Velocity	2000 ms^{-1}	1500 ms^{-1} to 60000 ms^{-1}
Grid space	$4m$	$5m$
Number of nodes	1000×1000	1200×700
Length and breadth	$4000m \times 4000m$	$6255m \times 3505m$
Figure number	6	7

Table 6: Specifications of the model

A two-dimensional snippet of the wave propagation in both models has been presented in Figure 6 and Figure 7, respectively. The Ricker wavelet (RT) has been used as a point source at any given time t for a frequency domain ω_0 is given by

$$R(t) = (1 - 2\pi^2 f_0^2 t^2) e^{-\pi^2 \omega_0^2 t^2} \tag{36}$$

A central frequency of $\omega_0 = 20HZ$ with appropriate zero time shift for the proper initial condition has been implemented during the simulation. To keep the stability conditions intact, the time steps have been taken as follows.

$$\frac{\Delta t}{h} c < \frac{2}{\sqrt{\Sigma_{i=-N}^{i=N} |A_i|}} \tag{37}$$

where, A_i denotes the coefficients of the finite difference operator. Although this criterion is commonly utilized for explicit schemes. However, as proxy criteria for the implicit schemes such as CCIFD as described in the paper, the above stability conditions may be employed.

The high accuracy and decreased numerical anisotropy can be attained at the cost of computational resources (in terms of memory used and CPU cycles). It occurs in explicit schemes because of the larger number of nodes that are calculated, but an implicit scheme needs a matrix inversion and node summation. Compared to the traditional finite difference approximations, the schemes presented here provide a better representation of the shorter length scales. According to a

theoretical FLOPS calculation, the implicit scheme CCIFD requires nearly twice as much time as CD8. This is because the nodes where the function values are prescribed are staggered from the nodes where the derivatives are evaluated by a half-cell (h/2). An inherent grid structure results from discretizing conservation equations with a finite volume. Although the CCIFD scheme's stencil's compactness is appealing, its use is limited by the cost of simulation. This feature preserves the flexibility in selecting the mesh geometry and boundary conditions while bringing them closer to the spectral methods. The work showcased here focuses more on the difference approximations' resolution properties than their formal accuracy (i.e., truncation error). By resolution characteristics, we mean the accuracy with which the difference approximation represents the exact result over the full range of length scales that can be realized on a given mesh. The numerical simulation clearly shows that, in comparison to conventional central difference schemes, the cell-centered scheme (CCIFD) considered here has better resolution characteristics for wavenumber near π.
To store matrices A and B of size $N \times N$, a significant amount of memory may be needed. By taking into account that A has a banded structure and B can be represented with a small number of elements, these requirements are lessened. According to a theoretical estimate of the accuracy of the FLOP count needed by various schemes, the 4^{th} order accurate cell-centered implicit derivative needs almost twice as many FLOPs as the conventional 8^{th} order CD operator. Though this scheme slightly overestimates the exact solution, its accuracy is optimum. Due to high-cost operations like recursion and division operators, the computational cost in time (simulation time) shows the opposite behavior. Although one may consider utilizing parallel algorithms to shorten the implicit scheme's computation time, the explicit parallel scheme is still more effective. For 2D and 3D models, the implicit scheme presented in this work exploits the pentadiagonal repetitive nature of matrix A. To further enhance performance, the LDMT decomposition is employed. The accuracy of the implicit scheme makes out for its slightly higher total expense compared to the explicit scheme. It would be worthwhile to highlight the boundaries at this point because they may also be a tiny source of error. The stencil exhibits symmetry and zero phase error at the interior region of a domain due to the equal number of nodes on both sides. Phase errors may be introduced by the boundary stencil because of its non-symmetric nature due to an uneven number of nodes on its sides. Because of the one-sided nature of the stencil, this effect cannot be avoided in a numerical scheme. However, compared to the CD scheme, the implicit scheme uses a lot fewer boundary points, so this effect is diminished. Additionally, since the effect is limited to a tiny area made up of only a few nodes, it can be disregarded. Furthermore, we discovered that the boundary conditions are easily applied and stable for the seismic wave simulation in acoustic media.

5. Conclusion

In this paper, we have introduced a Cell-Centered mesh, a compact scheme based efficient method for simulating acoustic waves. We have compared this compact scheme's accuracy in terms of the numerical derivative operator, the discretization-related phase velocity error, and the computational cost with those of several CD schemes of varying orders. It is to be noted that the fourth-order compact scheme has quite small differencing errors. This reveals that a cell-centered mesh compact scheme can provide almost exact second derivatives. However, the fourth-order pentadiagonal scheme slightly overpredicts the exact derivative. Higher-order cell-centered schemes are virtually indistinguishable from the exact differentiation. The locations of the minima and maxima for errors are similar across all schemes, including the implicit scheme. Compared to the lengthy explicit FD operator, this scheme has the advantage of smaller stencils that are more local in nature. Compared to the CD scheme, it requires fewer points even for boundary implementation, which results in less phase error. The computational cost of the 4th order CCIFD scheme is nearly twice that of the 8^{th} order explicit scheme for lower time steps, while it is almost equal for larger time steps, which can be readily extended from 1D to higher dimensions (2D/3D). By effectively simulating the wave propagation in 2D acoustic media (Homogeneous and Marmousi Model) using CCIFD, the applicability and stability of the scheme were shown. The cell-centered schemes can be easily constructed for interpolation and filtering applications. It can be useful to analyze operations in wavenumber (Fourier) space and may provide greater control over the shape of the transfer function (in the wavenumber space). The numerical scheme so presented maybe applied to the wave propagation in various composite media [36, 37].

Data and Resources

All data used in this paper came from published sources listed in the references.

References

[1] J. Carcione, Wave fields in real media: Wave propagation in anisotropic, anelastic, porous and electromagnetic media, Elsevier (2007).

[2] G. Seriani, S. Oliveira, Numerical modeling of mechanical wave propagation, La Rivista del Nuovo Cimento 49(8) (2020) 459–514.

[3] S. Kumawat, S. Praharaj, S. Vishwakarma, Dispersion of torsional surface waves in a threefold concentric compounded cylinder with imperfect interface, Waves in Random and Complex Media (2022) 1–26.

[4] S. Kumawat, S. Vishwakarma, Dynamic response of torsional waves in an anisotropic infinite cylinder with finite thickness, Physica Scripta 97 (11) (2022) 115004.

[5] A. Routa, P. Monahty, An improved reverse time migration for subsurface imaging over complex geological structures: A numerical study, Energy Geosci. 100239 (2023) 100239.

[6] J. Sun, K. Innanen, T. Zhang, D. Trad, Implicit seismic full waveform inversion with deep neural representation, J. Geophys. Res. Solid Earth 128(3) (2023).

[7] S. Venkateshan, S. P., Numerical Differentiation, Springer International Publishing, 2023.

[8] Z. Liu, P. Song, J. Li, J. Li, X. Zhang, An optimized implicit finite-difference scheme for the two-dimensional Helmholtz equation., Geophys. J. Int. 202(3) (2015) 1805–26.

[9] W. Zhang, Y. Zhuang, E. Chung, A new spectral finite volume method for elastic wave modelling on unstructured meshes, Geophys. J. Int. 206(1) (2016) 292–307.

[10] J. Virieux, H. Calandra, R. Plessix, A review of the spectral, pseudo-spectral, finite-difference and finite-element modelling techniques for geophysical imaging, Geophys. Prospect. 794-813 (2011).

[11] Z. Yang, X. Chen, Y. Xie, H. Zuo, H. Miao, X. Zhang, Wave motion analysis and modeling of membrane structures using the wavelet finite element method, Appl. Math. Model. 40(3) (2016) 2407–20.

[12] T. Maruyama, T. Saitoh, S. Hirose, Numerical study on sub-harmonic generation due to interior and surface breaking cracks with contact boundary conditions using time-domain boundary element method, Int J Solids Struct 1(126) (2017) 74–89.

[13] M. Taizo, S. Takahiro, S. H., 3-D Numerical simulation of sub-harmonic generation phenonmena due to contact acoustic nonlinearity on crack faces, J. Jpn. Soc. 72 (2016) I217–I226.

[14] J. Chen, J. Cao, Z. Li, A comparative study on the stress image and adaptive parameter-modified methods for implementing free surface boundary conditions in elastic wave numerical modeling, Geophys. 86(6) (2021) T451–67.

[15] N. Fan, L. Zhao, X. Xie, X. Tang, Z. Yao, A general optimal method for a 2D frequency-domain finite-difference solution of scalar wave equation, Geophys. 82(3) (2017) T121–32.

[16] E. Anthony, N. Vedanti, An optimized staggered-grid finite-difference operator for seismic wave simulation in poroelastic media, Geophys. 87(3) (2022) T225–36.

[17] A. Malkoti, N. Vedanti, R. Tiwari, An algorithm for fast elastic wave simulation using a vectorized finite difference operator, Comput and Geosci 1(116) (2018) 23–31.

[18] D. Kosloff, R. Pestana, H. Tal-Ezer, Acoustic and elastic numerical wave simulations by recursive spatial derivative operators, Geophys. 75 (2010) T167–T174.

[19] E. Wang, Y. Liu, M. Sen, Effective finite-difference modelling methods with 2-d acoustic wave equation using a combination of cross and rhombus stencils, Geophys. J. Int. 69(2) (2016) 1933–1958.

[20] R. Mittet, On the pseudospectral method and spectral accuracy, Geophys. 86(3) (2021) T127–42.

[21] J. Escolano, F. Jacobsen, J. J. López, An efficient realization of frequency dependent boundary conditions in an acoustic finite-difference time-domain model, J. sound vib. 316 (1-5) (2008) 234–247.

[22] B. Gosselin-Cliche, B. Giroux, 3D frequency-domain finite-difference viscoelastic-wave modeling using weighted average 27-point operators with optimal coefficients, Geophys. 79(3) (2014) T169–88.

[23] J. Flores, E. Salete, J. Benito, A. Vargas, E. Conde, Generalized finite difference method applied to solve seismic wave propagation problems, Math. Methods Appl. Sci. Geophys. (2023).

[24] K. K.R., R. Ward, S. Treitel, A. R.M., Synthetic seismograms: a finite difference approach, Geophys 41 (1976) 2–27.

[25] M. Dablain, The application of high-order differencing to the scalar wave equation., Math. Methods Appl. Sci. 51(1) (1986) 54–66.

[26] A. Malkoti, N. Vedanti, R. Tiwari, A highly efficient implicit finite difference scheme for acoustic wave propagation, Appl. Geophys. 1(161) (2019) 204–15.

[27] W. Zhou, D. Lumley, Central-difference time-lapse 4D seismic full-waveform inversion, Geophys. 86(2) (2021) R161–72.

[28] S. Lele, Compact finite difference schemes with spectral-like resolution, J. Comput. Phys. 103(1) (1992) 16–42.

[29] W. Zhou, D. Lumley, Central-difference time-lapse 4D seismic full-waveform inversion, Geophys. 86(2) (2021) R161–72.

[30] G. Ashcroft, X. Zhang, Optimized prefactored compact schemes, J. Comput. Phys. 190(2) (2003) 459–77.

[31] G. Ashcroft, X. Zhang, Prefactored optimized compact finite-difference schemes for second spatial derivatives, Geophys. 76(5) (2011) WB87–95.

[32] K. Li, W. Liao, An efficient and high accuracy finite-difference scheme for the acoustic wave equation in 3D heterogeneous media, J. Comput. Sci. 40 (2020) 101063.

[33] L. Chang, J. Stratton, H. Kim, W. Hwu, A scalable, numerically stable, high-performance tridiagonal solver using GPUs, Proc. of Int. Conf. High Perform. Comput. Netw. Storage Anal. (2012) 1–11.

[34] M. Nabavi, M. K. Siddiqui, J. Dargahi, A new 9-point sixth-order accurate compact finite-difference method for the helmholtz equation, J. Sound Vib. 307 (3-5) (2007) 972–982.

[35] A. Quarteroni, R. Sacco, F. Saleri, Numerical mathematics, Springer Science & Business Media & Business Media, 2010.

[36] S. Kumawat, S. Vishwakarma, Circumferential sh wave in piezo-reinforced composite structure with imperfect interface bonding, Applied Mathematical Modelling 123 (2023) 311–331.

[37] S. Kumawat, S. Vishwakarma, S. Althobaiti, A comparative study of reflection and refraction of sh waves across a tri-layered thin-walled microstructure, Thin-Walled Structures 192 (2023) 111166.

Appendix A. Central Difference Numerical Derivative

For order 2,

$$\begin{bmatrix}1&0&0&0&0\\0&1&0&0&0\\0&0&1&0&0\\0&0&0&1&0\\0&0&0&0&1\end{bmatrix}\begin{bmatrix}\phi_1''\\\phi_2''\\\phi_3''\\\phi_4''\\\phi_5''\end{bmatrix}=\frac{1}{h^2}\begin{bmatrix}-2&1&0&0&0\\1&-2&1&0&0\\0&1&-2&1&0\\0&0&1&-2&1\\0&0&0&1&-2\end{bmatrix}\begin{bmatrix}\phi_1\\\phi_2\\\phi_3\\\phi_4\\\phi_5\end{bmatrix}$$

For order 4,

$$\begin{bmatrix}1&0&0&0&0\\0&1&0&0&0\\0&0&1&0&0\\0&0&0&1&0\\0&0&0&0&1\end{bmatrix}\begin{bmatrix}\phi_1''\\\phi_2''\\\phi_3''\\\phi_4''\\\phi_5''\end{bmatrix}=\frac{1}{h^2}\begin{bmatrix}\frac{-5}{2}&\frac{4}{3}&\frac{-1}{12}&0&0\\\frac{4}{3}&\frac{-5}{2}&\frac{4}{3}&\frac{-1}{12}&0\\\frac{-1}{12}&\frac{4}{3}&\frac{-5}{2}&\frac{4}{3}&\frac{-1}{12}\\0&\frac{-1}{12}&\frac{4}{3}&\frac{-5}{2}&\frac{4}{3}\\0&0&\frac{-1}{12}&\frac{4}{3}&\frac{-5}{2}\end{bmatrix}\begin{bmatrix}\phi_1\\\phi_2\\\phi_3\\\phi_4\\\phi_5\end{bmatrix}$$

For order 6,

$$\begin{bmatrix}1&0&0&0&0\\0&1&0&0&0\\0&0&1&0&0\\0&0&0&1&0\\0&0&0&0&1\end{bmatrix}\begin{bmatrix}\phi_1''\\\phi_2''\\\phi_3''\\\phi_4''\\\phi_5''\end{bmatrix}=\frac{1}{h^2}\begin{bmatrix}\frac{-49}{18}&\frac{3}{2}&\frac{-3}{20}&\frac{1}{90}&0\\\frac{3}{2}&\frac{-49}{18}&\frac{3}{2}&\frac{-3}{20}&\frac{1}{90}\\\frac{-3}{20}&\frac{3}{2}&\frac{-49}{18}&\frac{3}{2}&\frac{-3}{20}\\\frac{1}{90}&\frac{-3}{20}&\frac{3}{2}&\frac{-49}{18}&\frac{3}{2}\\0&\frac{1}{90}&\frac{-3}{20}&\frac{3}{2}&\frac{-49}{18}\end{bmatrix}\begin{bmatrix}\phi_1\\\phi_2\\\phi_3\\\phi_4\\\phi_5\end{bmatrix}$$

For order 8,

$$\begin{bmatrix}1&0&0&0&0\\0&1&0&0&0\\0&0&1&0&0\\0&0&0&1&0\\0&0&0&0&1\end{bmatrix}\begin{bmatrix}\phi_1''\\\phi_2''\\\phi_3''\\\phi_4''\\\phi_5''\end{bmatrix}=\frac{1}{h^2}\begin{bmatrix}\frac{-205}{72}&\frac{8}{5}&\frac{-1}{5}&\frac{8}{315}&\frac{-1}{560}\\\frac{8}{5}&\frac{-205}{72}&\frac{8}{5}&\frac{-1}{5}&\frac{8}{315}\\\frac{-1}{5}&\frac{8}{5}&\frac{-205}{72}&\frac{8}{5}&\frac{-1}{5}\\\frac{8}{315}&\frac{-1}{5}&\frac{8}{5}&\frac{-205}{72}&\frac{8}{5}\\\frac{-1}{560}&\frac{8}{315}&\frac{-1}{5}&\frac{8}{5}&\frac{-205}{72}\end{bmatrix}\begin{bmatrix}\phi_1\\\phi_2\\\phi_3\\\phi_4\\\phi_5\end{bmatrix}$$

Appendix B. Matrix A and B for CCIFD

$$A = \begin{bmatrix}1&0&-80.105&0&0&0&0&0&0\\0&1&0&-24.777&0&0&0&0&0\\-0.012&0&1&0&0&0&0&0&0\\0&-0.333&0&1&0&-0.333&0&0&0\\0&0&-0.333&0&1&0&-0.333&0&0\\0&0&0&-0.333&0&1&0&-0.333&0\\0&0&0&0&0&0&1&0&-0.012\\0&0&0&0&0&-24.777&0&1&0\\0&0&0&0&0&0&-80.105&0&1\end{bmatrix},$$

$$B = \begin{bmatrix}10.007&-116.745&209.404&-105.043&-3.743&9.464&-4.225&0.980&-0.098\\0.417&3.388&-40.077&72.622&-41.416&5.938&-0.986&0.121&-0.007\\-0.124&1.457&-2.611&1.291&0.082&-0.138&0.055&-0.012&0.001\\2.5&0&-10.5&16&-10.5&0&2.5&0&0\\0&2.5&0&-10.5&16&-10.5&0&2.5&0\\0&0&2.5&0&-10.5&16&-10.5&0&2.5\\0.001&-0.012&0.055&-0.138&0.082&1.291&-2.611&1.457&-0.124\\-0.007&0.121&-0.986&5.938&-41.416&72.622&-40.077&3.388&0.417\\-0.098&0.980&-4.225&9.464&-3.743&-105.043&209.404&-116.745&10.007\end{bmatrix} \quad \text{(B.1)}$$

Appendix C. Description of the LDM^T decomposition:

The matrix A is decomposed as follows,

$$A = LDM^T \quad \text{(C.1)}$$

$$
\begin{bmatrix}
a_1 & c_1 & d_1 & 0 & \cdots & 0 & 0 \\
b_2 & a_2 & c_2 & d_2 & \cdots & 0 & 0 \\
e_3 & b_3 & a_3 & c_3 & d_3 & 0 & 0 \\
\vdots & \vdots & & \ddots & & & \vdots \\
 & & & & \ddots & & d_{n-2} \\
0 & 0 & \cdots & & & c_{n-1} & \\
0 & 0 & \cdots & & e_n & b_n & a_n
\end{bmatrix}
=
\begin{bmatrix}
\zeta_1^{-1} & 0 & 0 & 0 & \cdots & 0 & 0 \\
\phi_2 & \zeta_2^{-1} & 0 & 0 & \cdots & 0 & 0 \\
e_3 & \phi_3 & \zeta_3^{-1} & 0 & \cdots & 0 & 0 \\
\vdots & \vdots & & \ddots & & & \vdots \\
 & & & & \ddots & & 0 \\
0 & 0 & \cdots & & & \phi_n & \zeta_n^{-1}
\end{bmatrix}
\begin{bmatrix}
\zeta_1 & 0 & 0 & 0 & \cdots & 0 & 0 \\
0 & \zeta_2 & 0 & 0 & \cdots & 0 & 0 \\
0 & 0 & \zeta_3 & 0 & \cdots & 0 & 0 \\
\vdots & \vdots & & \ddots & & & \vdots \\
 & & & & \ddots & & 0 \\
0 & 0 & \cdots & & & \zeta_n &
\end{bmatrix}
\begin{bmatrix}
\zeta_1^{-1} & \psi_1 & s_1 & 0 & \cdots & 0 & 0 \\
0 & \zeta_2^{-1} & \psi_2 & s_2 & \cdots & 0 & 0 \\
0 & 0 & \zeta_3^{-1} & \psi_3 & \cdots & 0 & 0 \\
\vdots & \vdots & & \ddots & & & \vdots \\
 & & & & \ddots & & s_{n-1} \\
 & & & & & \ddots & \psi_{n-1} \\
0 & 0 & \cdots & & & 0 & \zeta_n^{-1}
\end{bmatrix}
$$

where,

$$
\zeta_i = \begin{cases} a_1^{-1} & \text{if } i = 1 \\ (a_2 - \phi_2\zeta_1\psi_1)^{-1} & \text{if } i = 2 \\ (a_i - e_i\zeta_{i-2}s_{i-2} + \zeta_{i-1}\psi_{i-1}\phi_i)^{-1} & \text{if } i = 3, 4, \ldots n \end{cases} \tag{C.2}
$$

$$
\phi_i = \begin{cases} b_2 & \text{if } i = 2 \\ b_i - e_i\zeta_{i-2}\psi_{i-2} & \text{if } i = 3, 4, \ldots n \end{cases} \tag{C.3}
$$

$$
\psi_i = \begin{cases} c_1 & \text{if } i = 1 \\ c_i - \zeta_{i-1}s_{i-1}\phi_i & \text{if } i = 2, 4, \ldots n-1 \end{cases} \tag{C.4}
$$

Algorithm to solve the 1D problem:

1) Calculate the system, $A\phi'' = B\phi$ for 1D.

2) Break down the constant matrix A into LDM^T as shown above.

3) Calculate the vector ζ.

4) To get the decomposition in higher dimension, 1D process can be used iteratively.

Highlights:

1. Cell-Centered Implicit Finite Difference (CCIFD) scheme is discussed.
2. Spectral analysis is performed.
3. Error and anisotropy of CCIFD scheme is discussed.
4. CPU time for LU and LDMT decomposition is calculated and compared.
5. Numerical simulation is conducted in Homogeneous and Marmousi model.

Declaration of interests

1. Declaration of interests

☑ The authors declare that they have no known competing financial interests or personal relationships that could have appeared to influence the work reported in this paper.

☐The authors declare the following financial interests/personal relationships which may be considered as potential competing interests:

2. Contributions

☑ Each author declares substantial contributions through the following:
(1) the conception and design of the study, or acquisition of data, or analysis and interpretation of data,
(2) drafting the article or revising it critically for important intellectual content,

Please indicate for each author the author contributions in the text field below. Signatures are not required.

Sunita Kumawat has formulated the problem, derived the solution, interpretation of results, drafted the article.
Sunita Kumawat and Ajay Malkoti has plotted the graphs and carried out the simulations.
Sumit Kumar Vishwakarma has carried out the Computation part , numerical discussion and helped in revising the article with intellectual content.

3. Approval of the submitted version of the manuscript

☑ Please check this box to confirm that all co-authors have read and approved the version of the manuscript that is submitted. Signatures are not required.